Pol. J. Environ. Stud. Vol. XX, No. X (XXXX), 1-19
DOI: *10.15244/pjoes/210365* ONLINE PUBLICATION DATE: 2025-12-03

Original Research

Research on the Calculation Method of Carbon Emissions Integrating Nighttime Lighting Data and the Coefficient of Urban Industrial Structure Level

Wenfeng Huang[1], Xiaoyu Zhang[2]°*, Ke Pan[2], Jie Luo[3], Hao Tang[2]

[1]Geomathematics Key Laboratory of Sichuan Province, Chengdu University of Technology, Chengdu 610059, China
[2]School of Mathematical Sciences, Chengdu University of Technology, Chengdu 610059, China
[3]Chengdu College of Arts and Sciences, Chengdu 610401, China

Received: 31 March 2025
Accepted: 5 September 2025

Abstract

Amid the global challenge of carbon emissions (CE), developing a method for accurately measuring city-level carbon emissions is crucial for crafting effective carbon reduction strategies. Therefore, the integration of urban nighttime light data (NTL) and urban industrial structure (IS) characteristics contributes to the characterization of urban carbon emissions. It uses the ISC to reflect urban industrial structure variances across 21 cities and counties in Sichuan Province, establishing a correlation between NTL-ISC and urban carbon emissions through a PSO-SVM model. This approach is evaluated against the conventional NTL method, aiming for precise urban CE quantification. Additionally, the impact of the tertiary sector, population density, and urbanization on CEI and CEC is analyzed. Findings indicate: (1) A comparison between the traditional linear regression method, solely based on NTL (adjusted $R^2 = 0.86$), and the machine learning method incorporating NTL-ISC (adjusted $R^2 = 0.89$), demonstrates the efficacy of the proposed carbon emission measurement methodology. (2) Population density exhibits divergent contribution rates to cities with medium and low IS, with the tertiary industry's impact inversely related to population density. The urbanization rate significantly affects Panzhihua. This study enhances and broadens the methodologies for measuring urban carbon emissions using NTL, offering support for cities of varied industrial structures in devising tailored carbon reduction policies.

Keywords: urban carbon emission, NTL, industrial structure, PSO-SVM

Introduction

Since the 21st century, rapid urbanization and the pressing challenge of climate change have emerged as two interconnected core issues on the global sustainable development agenda. Cities, serving as hubs for economic activity, population concentration, technological innovation, and energy consumption, play a pivotal role in driving global carbon emissions [1]. Statistics indicate that urban areas account for 80% of global GDP, consume 60-80% of the world's energy, and contribute to 75% of total carbon emissions [2].

*e-mail: zxyu0207@163.com
°ORCID iD: 0009-0000-7540-5211

This global trend is particularly pronounced in China, where the urbanization rate surged from 42.99% in 2005 to 63.89% in 2020, reflecting an ongoing phase of rapid urban expansion that inevitably exacerbates environmental pollution, land scarcity, and industrial restructuring challenges [3, 4]. Moreover, urban carbon emissions in China constitute 85% of the nation's total – a figure significantly higher than that of developed economies such as the United States (80%) and Europe (69%) – underscoring the immense decarbonization pressure driven by concurrent industrialization and urbanization [5, 6]. Consequently, achieving accurate, efficient, and high-spatial-resolution measurement of urban-scale carbon emissions is not only the foundational step for assessing urban sustainability and environmental impact but also a critical scientific basis for China to implement its "dual carbon" strategy, balancing regional economic growth with ecological conservation.

Precise quantification of urban carbon emissions remains a complex scientific challenge. Traditional accounting methods primarily follow two technical pathways: top-down and bottom-up. The former allocates regional or national energy statistics to urban units using proxies like GDP or population, offering simplicity but suffering from low spatial resolution and an inability to capture intra-city emission disparities [7]. The latter aggregates activity data from various emission sectors within cities, yielding higher accuracy but demanding extensive data inputs, incurring high costs, and struggling to enable large-scale, long-term dynamic monitoring [8]. Recent advances in remote sensing, particularly the advent of NTL data, have revolutionized the monitoring of human activity and spatial dynamics across scales and time, effectively addressing gaps in statistical data. Rich in information, NTL data serve as a robust proxy for urbanization [9], economic development [10], and population density [11], and have been widely applied to CO_2 emission modeling [12]. Early studies relied on linear regression to directly correlate NTL luminosity with officially reported carbon emissions for spatial downscaling [13]. However, such simplistic linear relationships fail to capture real-world complexities – for instance, sensor saturation in urban cores masks further economic growth. To overcome these limitations, subsequent research introduced sophisticated nonlinear models, including quadratic polynomials [14], logistic functions, and machine learning algorithms (e.g., support vector machines, random forests, and artificial neural networks), which demonstrate superior accuracy in deciphering the intricate NTL-emission relationship [15]. Concurrently, data sources have evolved from DMSP/OLS to NPP/VIIRS, offering higher spatial resolution, broader dynamic range, and saturation-free detection [16], thereby enhancing estimation potential.

However, despite continuous optimization of models and data, existing research generally assumes the relationship between NTL and carbon emissions within the study region to be "spatially homogeneous". This implies that once a model is trained, its fitted parameters are applied uniformly across all units within the region [17]. This assumption overlooks the diverse development patterns of cities. Cities are not isolated, homogeneous points; instead, they are complex systems with significant heterogeneity. There are marked differences among cities in industrial structure, technology levels, energy consumption patterns, and urban morphology [18]. Consequently, this assumption of homogeneity inevitably introduces systematic errors. Particularly in regions with diversified industrial structures, it tends to seriously overestimate carbon emissions of service-oriented cities and underestimate those of industrial-oriented cities [19], which greatly undermines the accuracy of the estimation results and their reliability as a basis for policy-making.

Industrial structure, a fundamental force in shaping urban economic geography and determining energy consumption characteristics, is thus a key driver of urban carbon emission differences [20]. With the rapid development of urban economies and the increase in industrialization levels, the proportion of the secondary industry has risen sharply. This extensive development model has led to significant resource consumption and greenhouse gas emissions. The potential of urban industrial structural transformation to alleviate energy consumption and CO_2 emissions has been extensively studied. Currently, methods such as structural decomposition analysis, input-output models, and econometric analysis are commonly used to study the impact of industrial structural changes on CO_2 emissions. For example, Zeng et al., using a spatial difference-in-differences method, analyzed the impact mechanism of the Low-Carbon City Pilot Policy (LCCP) and found that industrial structure optimization and urban innovation can significantly reduce carbon emission intensity [21]. Wang et al., through the STIRPAT model, demonstrated that economic agglomeration and industrial structure have a significant impact on urban carbon emission efficiency [13]. Li et al. developed a model of the impact of industrial structural changes on urban carbon emissions, showing that industrial agglomeration and optimization can effectively alter urban carbon emissions [22].

Moreover, industrial structure optimization helps improve resource allocation among the three industrial sectors, enhances technological levels, modifies energy consumption structures, and consequently reduces urban CO_2 emissions (Fig. 1). The production processes of the secondary industry are highly dependent on fossil fuels, making it both energy-intensive and carbon-intensive. In contrast, the tertiary industry exhibits significantly lower energy consumption and carbon emission intensity per unit output value compared to the secondary industry [23]. Therefore, the transition from secondary to tertiary industries in urban areas directly leads to improved overall energy efficiency and reduced carbon emission intensity. Furthermore, industrial upgrading brings technological progress

and optimized resource allocation. Different industrial structures typically possess varying technological levels and innovation capacities, which can comprehensively enhance energy efficiency in social production through measures such as promoting energy-saving equipment and developing clean energy technologies [24]. Simultaneously, production factors, including capital and labor, shift from traditional high-pollution, high-energy-consumption sectors to cleaner and more efficient modern service industries and high-tech industries, achieving optimized resource allocation across society [25]. Although the decisive role of industrial structure in carbon emissions has become an academic consensus [26], current macro-level analyses of industrial structure impacts remain disconnected from micro-scale NTL-based spatial estimations. While NTL-based remote sensing studies pursue spatial precision, they overlook industrial structure as a key socioeconomic factor. Conversely, macro-level industrial structure research fails to provide refined spatial emission inventories. This disconnection significantly limits the explanatory power and predictive capability of existing carbon emission estimation models.

The core objective of this paper is to incorporate the industrial structure as a quantitative factor into the remote sensing estimation model, thereby constructing a new framework for urban carbon emission measurement that considers both accuracy and spatial characteristics simultaneously. This paper, aiming at the heterogeneity of the industrial structure in cities, constructs an ISC that integrates multiple dimensions such as output value structure, employment ratio, and labor productivity. On this basis, ISC is taken as the key explanatory variable and integrated together with the NTL data into the PSO-SVM model of particle swarm optimization, thereby effectively overcoming the limitations of the traditional linear model and correcting the homogeneity assumption bias caused by relying only on NTL. The organizational structure of this article is as follows: The first part provides an overview of the current research status of carbon emission measurement at the urban level; The second part briefly introduces the research framework of this paper; The third part introduces the data sources and constructs an urban carbon emission measurement model integrating NTL and ISC; The fourth part is mainly about the results; The fifth part and the sixth part are discussion and conclusion.

Framework

Based on the perspective of city-scale CE measurement, this paper proposes a method predicated on ISC and NTL, factoring in city-specific NTL and industrial structure level disparities. Initially, we construct the city industrial structure evaluation index system, employing the Entropy Weight Method (EWM) to secure the weight-age of each index, with a weighted average yielding the industrial structure level coefficient for each city. Subsequently, we use PSO-SVM to quantify the nonlinear relationship between city-scale CE and NTL, ISC, comparing these outcomes with traditional regression methods. Lastly, we quantify the contribution rates of the tertiary industry, urbanization, and population density to city CEI and CEC (Fig. 2).

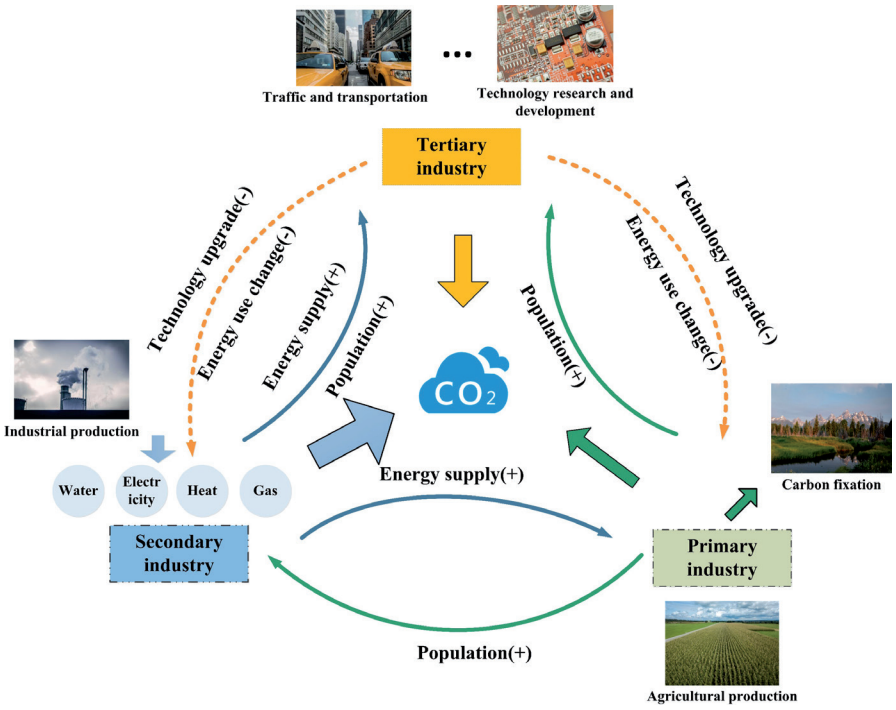

Fig. 1. Effect of industrial structure optimization on carbon emission.

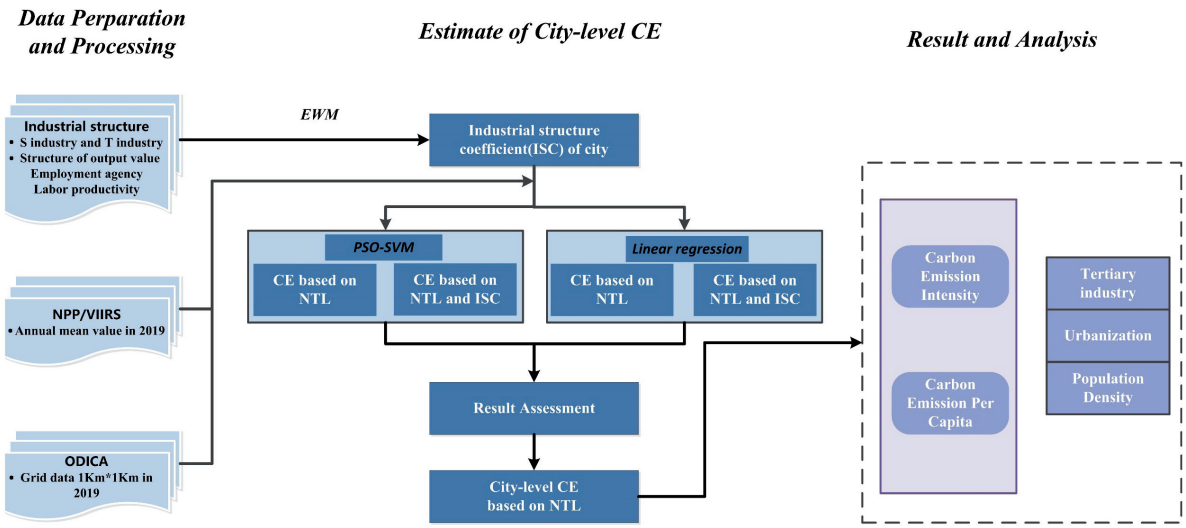

Fig. 2. Framework of study.

(1) Construct the evaluation index system of the city industrial structure. We begin by constructing an evaluation index system for city industrial structures, selecting six pertinent indices, including the output value proportion, the number of employees, and labor productivity within both secondary and tertiary industries. We employ the EWM to derive the respective index weights, enabling us to ascertain a weighted average ISC.

(2) City-scale CE measurement method. We propose a method to measure city-scale CE. We establish a relationship between city NTL, ISC, and city-scale CE using both traditional regression models and the PSO-SVM. The computed results of these two models are then compared and analyzed.

(3) Contribution rates of CEI and CEC in cities. We evaluate the contribution rates of CEI and CEC in various cities. We compile data on the proportion of the tertiary industry, urbanization rates, and population density across 21 cities. Taking into account the overall difference level of impact factors on CEI and CEC, we calculate the relative contribution rate of these impact factors, and analyze their effect on CEI and CEC across different cities.

Materials and Methods

Study Area

This paper focuses on Sichuan Province (26°03'~34°19', 97°21'~108°12), covering a sprawling area of 486,000 Km^2 and governing 21 prefecture-level administrative regions, including 18 prefecture-level cities and 3 autonomous prefectures. Fig. 3 illustrates the spatial distribution of this region. As a dominant economic province in western China, Sichuan boasts rich resources and a substantial population. Prior to 2019, Sichuan underwent a period of rapid economic growth, experiencing considerable alterations in the three industrial structures. Concurrently, the burgeoning level of industrialization caused a rise in the secondary industry's proportion, which consequently led to increased emissions of CO_2 and other greenhouse gases. Given the differences in industrial structure level across cities, accurate city-scale carbon emission measurements and research on spatial CE characteristics are instrumental in aiding government bodies to reasonably formulate pertinent emission reduction policies.

The Coefficient of the Industrial Structure Level

According to the industrial indicators of cities in 2019, the EWM is used to calculate the ISC of 21 cities in Sichuan province and quantify the characteristics of the industrial structure of cities. The evaluation of the characteristics of regional industrial structure requires that it can reflect the situation of the city industrial structure more comprehensively and reflect the characteristics of urban structure as much as possible through the evaluation index. Based on the above principles, this paper selects three dimensions of industrial structure, employment structure, and labor productivity (Table 1) to construct the ISC. Among them, the output value structure and employment structure can well depict the differences in industrial structure among cities. The dimension of labor productivity can reflect the internal upgrading of the industry and the depth of industrial upgrading to make up for the deficiency of the evaluation dimension of industrial structure and employment structure. Given that both secondary and tertiary industries profoundly affect city-scale CE and substantially influence the industrial structure level, the paper incorporates the output value ratio (output value structure), the employment number ratio (employment structure), and labor productivity as industrial structure

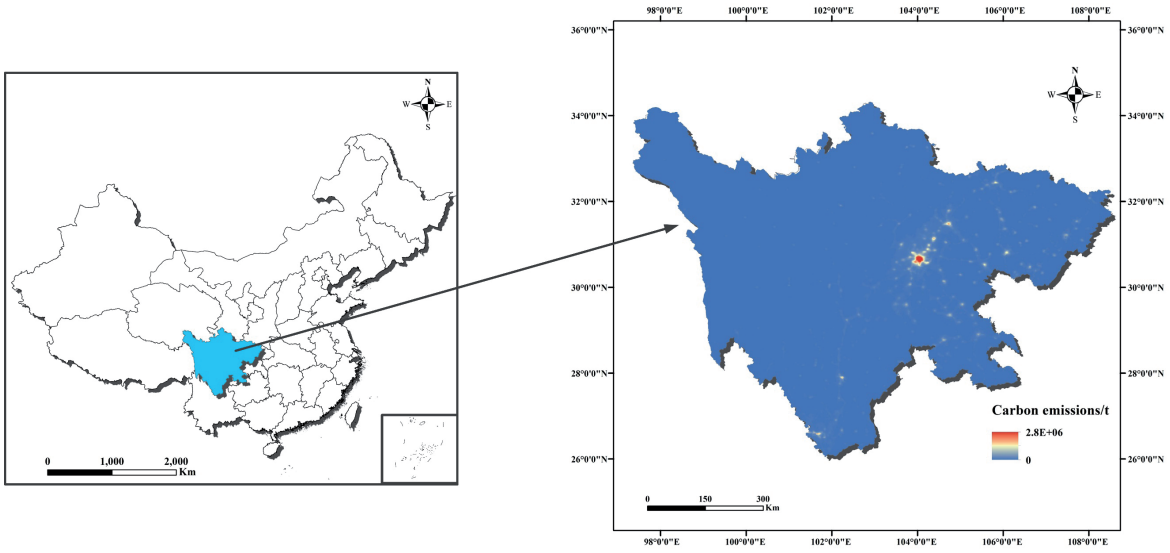

Fig. 3. Spatial distribution of the study areas and distribution characteristics of CE.

evaluation indices [27, 28]. Throughout this paper, all of the indicators selected are positive indicators, and no positive processing is performed on them.

The EWM [29] is utilized to quantify the Shannon entropy of each indicator, which in turn yields a comprehensive weight for each indicator. The city ISC is obtained by a weighted average of the indicators:

$$\mathrm{ISC} = \sum_{i=1}^{n} w_i I_i \tag{1}$$

Where, ISC represents the coefficient of the industrial structure level of a city. w_i represents the weight obtained by EWM. I_i represents the *i-th* index value. The details are shown in Table 1.

Data and Preprocessing

Given the scale of energy data, procuring city-scale energy consumption data is a challenging task. Therefore, we adopted the Open-source Data Inventory for Anthropogenic CO_2 (ODIAC) spatial data on city-scale CE furnished by the Institute of Public and Environmental Affairs (IPE) [Source: https://db.cger.nies.go.jp/]. ODIAC offers a global high-resolution grid with a spatial resolution of 1 km×1 km. We collected the NPP/VIIRS nighttime light data for 12 months in 2019 and 2020. According to the study area, we cropped the nighttime light images of Sichuan province using ArcGIS software, resampled them into a 1 km×1 km raster, and calculated the annual average values of the nighttime light data in 2019 and 2020. Based on the administrative divisions of 21 cities (prefectures) in Sichuan province, we obtained the annual average values of night lights in Sichuan province in 2019 and 2020 by cutting

Table 1. Specific description of indicators.

Dimensions	Specific indicators	Formula	Weight
Industrial structure	Proportion of secondary industry GDP	$GDP_{s,i} / GDP_{Total,i}$	0.14
	Proportion of tertiary industry GDP	$GDP_{t,i} / GDP_{Total,i}$	0.17
Employment structure	Proportion of employment in the secondary industry	$EP_{s,i} / EP_{Total,i}$	0.07
	Proportion of employment in the tertiary industry	$EP_{t,i} / EP_{Total,i}$	0.17
Labor productivity	Labor productivity in the secondary industry	$GDP_{s,i} / EP_{s,i}$	0.24
	Labor productivity in the tertiary industry	$GDP_{t,i} / EP_{t,i}$	0.21

and summing. (The night light data used in this paper are all annual averages, which can comprehensively reflect the situation of night lights in a certain area within a year.) The NPP/VIIRS nighttime light data have background noise caused by low-radiation detection. The DN values of these noise points are negative. To ensure the normal progress of subsequent studies, in this paper, we replaced the negative DN values with 0 values. In the NPP/VIIRS nighttime light data, there are also extremely bright pixel values caused by the instantaneous field of view, and their DN values are usually much higher than other DN values. In this paper, we take the central point DN value of Chengdu, the most economically developed area in Sichuan province, as the highest DN value within Sichuan province, and remove the pixel points with DN values much greater than this value. We carry out operations such as summation and research area cropping in the ArcGIS software to obtain the CE data of Sichuan province in 2019, and statistically analyze the sum of pixel values of each city to obtain the CE data of each of the 21 cities. Additionally, data on each city's GDP ratio of the secondary and tertiary industry, employment ratio, and labor productivity were sourced from the 2019 Sichuan Statistical Yearbook [Source: http://tjj.sc.gov.cn/]. NTL data were retrieved from NPP/VIIRS images [Source: https://eogdata.mines.edu/products/vnl/], with the annual average calculated from the collected monthly NPP/VIIRS data for 2019.

Methodology

Linear Regression

Current methodologies for measuring city-scale CE largely rely on unitary linear regression models, using NTL values and statistical city-scale CE. This method assumes that the linear relationship between NTL and CE is constant within a specific province [13]. Therefore, city-scale CE are calculated by consistent fitting coefficient and NTL for cities in provinces [16, 30], but this measurement method tends to overestimate or underestimate city-scale CE [31]. Previous studies have pointed out that the industrial structure of a city may have an impact on the regression model [24]. Therefore, on the basis of NTL, this paper combined the level of city industrial structure to measure city-scale CE. The linear regression model for city-scale CE is as follows:

$$\mathrm{CE}_i = \alpha_1 NTL_i + \alpha_2 ISC_i + \alpha_0 + \varepsilon \tag{2}$$

Where, CE_i represents the computed CE value for the *i-th* city, NTL_i and ISC_i represent the night light value of a city, and the ISC, respectively. α_0 represents the intercept term, and ε represents the error term.

PSO-SVM

Traditional linear regression models, when compared with machine learning methods, encounter difficulties in achieving precise CE measurements. Research by Yang et al. has demonstrated the effectiveness of machine learning in enhancing NTL-based CE measurement [32]. Given the Support Vector Machine (SVM) model's proficiency in learning from small samples and the Particle Swarm Optimization (PSO) algorithm's superior global optimization capabilities, the PSO-SVM algorithm is adopted to construct a functional mapping relationship between NTL-ISC and city-scale CE, facilitating precise measurements of city-scale CE. Support Vector Machine (SVM) is a supervised learning algorithm based on structural risk minimization theory. Its decision boundary is the maximum margin hyperplane to solve the learning sample. It can transform the problem into a convex quadratic programming problem. SVM provides a clearer and more powerful way to learn complex nonlinear equations. The specific steps are as follows:

$$f(x) = \omega\psi(x) + b \tag{3}$$

Where $\psi(x)$ represents the mapping function, ω and b represent the weights and deviations, respectively. The calculation of the SVM model can be derived by employing the insensitive loss function ε to solve the following convex optimization problems:

$$\begin{cases} minimize \dfrac{1}{2}\|\omega\|^2 + c\left[\sum_{i=1}^{N}(\xi_i + \xi_i^*)\right] \\ \omega\phi(x_i) + b - y_i \le \varepsilon + \xi_i^*, i = 1,2,\cdots,N \\ y_i - \omega\phi(x_i) - b \le \varepsilon + \xi_i, i = 1,2,\cdots,N \\ \xi, \xi_i^*, i = 1,2,\cdots,N \end{cases} \tag{4}$$

Where c represents the positive parameter used to control the empirical error, ξ_i and ξ_i^* represent the relaxation variables used to control the training error. x_i and y_i represent input and output variables, respectively. N represents the number of samples.

Given the impact of the optimal penalty parameter c, kernel function parameter g, and kernel function ∂ on regression results, the particle swarm optimization algorithm (PSO) [33] was used to optimize SVM. As a random search method, PSO can realize individual optimization in space. The position and velocity of the *i-th* particle are expressed by Equations (5) and (6), respectively.

$$X_i^{k+1} = X_i^k + V_i^{k+1} \tag{5}$$

$$V_i^{k+1} = \omega V_i^k + c_1 r_1 (P_i^k - X_i^k) + c_2 r_2 (g^k - X_i^k) \tag{6}$$

Where, ω, c_1 and c_2 respectively represent inertia weight, acceleration factor 1 and acceleration factor 2. r_1 and r_2 represent random numbers distributed in [0,1]. k represents the number of current iterations.

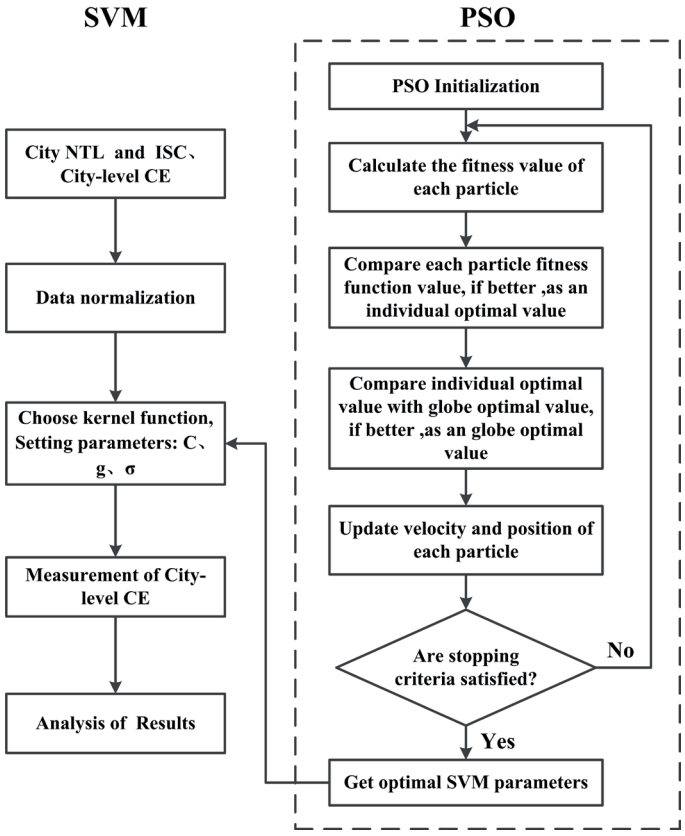

Fig. 4. Measurement model of city-scale CE based on PSO-SVM.

V_i represents the velocity of the *i-th* particle. P_i^k is the personal optimal position at the *k-th* update. g^k represents the global optimal position at the *k-th* update. Detailed optimization steps are shown in Fig. 4.

The specific settings of the corresponding parameters of the particle swarm optimization algorithm in this paper are as described in Table 2.

Global Moran Index

The spatial autocorrelation analysis method is a way to determine whether it has spatial origin. This measurement method is determined by measuring whether regions in close proximity have similar variable values. The Moran index is an important statistical tool, mainly used to measure the existence of spatial autocorrelation in spatial data, thereby revealing the spatial aggregation phenomenon of data. If high values cluster together with high values and low values cluster together with low values, it is "positive spatial autocorrelation". Conversely, if a high value is adjacent to a low value, it is called "negative space autocorrelation". If the high values and low values are randomly distributed, there is no spatial autocorrelation. The Moran index is divided into the global Moran index (I_G) and the local Moran index (I_L), which are respectively used to analyze different spatial correlation characteristics.

Table 2. Particle swarm parameter setting.

Parameters	Value
Maximum number of iterations	20
Particle swarm size *n*	50
Local search ability c_1	1.5
Global search ability c_2	1.5
The search range of *c*	(0,1500)
The search range of *g*	(0,1500)

The global Moran index is used to comprehensively analyze the autocorrelation in the overall space, helping to identify the spatial effects and trends in the entire spatial sequence, and can reveal whether there are significant spatial aggregation or dispersion patterns in the entire region. Its calculation formula is:

$$I = \frac{n\sum_{i=1}^{n}\sum_{j=1}^{n} w_{ij}(x_i - \bar{x})(x_j - \bar{x})}{\sum_{i=1}^{n}\sum_{j=1}^{n} w_{ij}\sum_{i=1}^{n}(x_i - \bar{x})^2} \quad (7)$$

In the formula, x_i and x_j respectively represent the carbon emission levels of city (prefecture) i and city (prefecture) j. $\bar{x}$ represents the average carbon emission level of all cities (states) in that year. n represents

the number of 21 cities (prefectures) in Sichuan Province. w_{ij} represents the value of the *i-th* row and *j-th* column in the spatial weight matrix. In this paper, the geographical adjacency matrix is adopted as the spatial weight matrix. It takes whether two places are adjacent as the value criterion. If two provinces are adjacent, then $w_{ij} = 1$; otherwise, $w_{ij} = 0$.

Contribution Rates of Factors to CEI and CEC

The computation processes of CEI and CEC are shown in Equations (8) and (9):

$$CEI = CE / GDP \tag{8}$$

$$CEC = CE / POP \tag{9}$$

The global CEI and CEC in 2019 were approximately 0.064 t/10,000 yuan and 4.4 t/person, respectively [34]. The CEI and CEC of Sichuan Province were 0.13 t/10,000 yuan and 0.75 t/person, respectively. Past research has highlighted the impact of the tertiary industry, urbanization, and population density on CEI and CEC; comprehensive studies on the degree of these three factors' impact remain scarce. Therefore, this paper conducts a quantitative study on the contribution of the tertiary industry, urbanization, and population density to CEI and CEC. In this regard, Formulas (10) and (11) [35] are used to quantify the relative contribution rate of a certain factor level to the overall difference between CEI and CEC:

$$K^i_{cei} = \frac{G_i}{\sum G_i} \times \frac{CEI_i - GCEI}{\overline{CEI} - GCEI} \tag{10}$$

$$K^i_{cec} = \frac{P_i}{\sum P_i} \times \frac{CEC_i - GCEC}{\overline{CEC} - GCEC} \tag{11}$$

Where, K^i_{cei} represents the CEI difference among cities, and K^i_{cec} represents the CEC difference of cities. *GCEI* and *GCEC* represent the global CEI and CEC in 2019, which are 0.064 t/10,000 yuan and 4.4 t/person, respectively. $\frac{CEI_i - GCEI}{\overline{CEI} - GCEI}$ represents the relative value of the difference between each city's CEI and Sichuan Province's CEI. $\frac{CEC_i - GCEC}{\overline{CEC} - GCEC}$ represents the relative value of the difference between each city's CEC and Sichuan Province's CEC. $\frac{G_i}{\sum G_i}$ and $\frac{P_i}{\sum P_i}$ respectively represent the relative horizontal weights of GDP and population of the *i-th* city with respect to the GDP and population of Sichuan Province.

Based on the difference coefficient attained through Formulas (12) and (13), the contribution rate of each factor is presented as follows:

$$C^i_{cei} = \frac{V_{fi} / M_f \times K^i_{cei}}{\sum_{i=1} V_{fi} / M_f \times K^i_{cei}} \tag{12}$$

$$C^i_{cec} = \frac{V_{fi} / M_f \times K^i_{cec}}{\sum_{i=1} V_{fi} / M_f \times K^i_{cec}} \tag{13}$$

Where, C^i_{cei} and C^i_{cec} represent the relative contribution rate of the *f-th* factor to the CEI difference and CEC difference of the *i-th* city, respectively. V_{fi} represents the value of the *f-th* factor of the *i-th* city; M_f represents the overall value of the *f-th* factor in Sichuan Province.

Results

City Industrial Structure Level and Characteristics of City-Scale Carbon Emissions

According to the measurement method of ISC (see Table 1 for specific rights), the coefficients of industrial structure of 21 cities are calculated, as shown in Fig. 5. The industrial structure level of Sichuan Province is uneven. Chengdu and Panzhihua showcase significantly higher ISC coefficients compared to the other cities. Only 7 cities, namely Chengdu, Panzhihua, Deyang, Leshan, and Ganzi, exceed the overall average of 0.36. Additionally, most cities fall within the 0.27 (lower quartile) and 0.43 (upper quartile) range, further underscoring the marked heterogeneity in Sichuan Province's industrial structure level, with the majority of cities' industrial structures situated at a low to medium level.

Fig. 5 indicates Chengdu and Panzhihua have ISC values of 0.74 and 0.63, respectively, significantly outpacing other cities. Ziyang, on the other hand, has the lowest ISC value of 0.20 among the 21 cities. Chengdu is the political, economic, and cultural center of Sichuan Province. As the fastest developing city in western China in recent years, it has a solid foundation of scientific research and technological innovation resources, and the tertiary industry occupies an absolutely dominant position in its industrial structure, leading to a significantly higher level of industrial structure than other cities. As an industrial city, Panzhihua has a relatively complete industrial system and is an important export city of mineral resources in western China. In recent years, its industrial structure has been gradually optimized, and it is transforming to the tertiary industry. Ziyang, conversely, despite its abundant agricultural resources, lacks economic scale, yielding a weaker economic base and correspondingly low ISC.

In 2019, CE from fossil energy consumption in 21 cities of Sichuan Province approximated 0.615 billion tons. The spatial distribution pattern of CE displayed

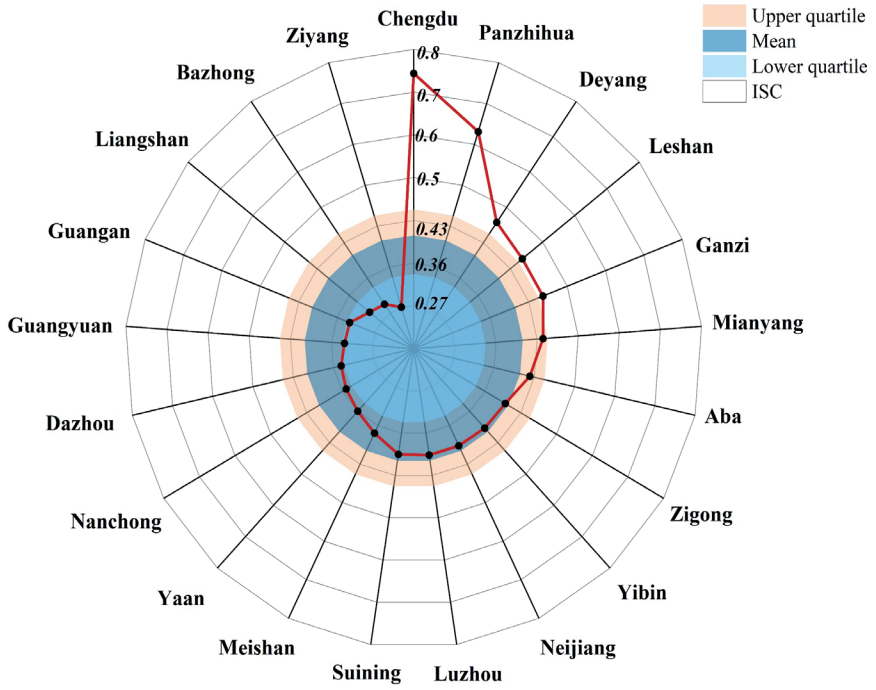

Fig. 5. Coefficient of the industrial structure level of cities.

a higher concentration in the east compared to the west (Fig. 6), indicating significant spatial heterogeneity of CE within Sichuan Province.

According to the variance in ISC across the 21 cities, cities are categorized into three distinct groups: Advanced Industrial Structure (Advanced-IS) cities (>0.46), Medium Industrial Structure (Medium-IS) cities (0.31-0.46), and Low Industrial Structure (Low-IS) cities (<0.31). It is evident that both Advanced-IS cities and Medium-IS cities primarily cluster in the southern and northwestern regions of Sichuan (Fig. 6). The average CE of the three cities are 1 million tons, 0.2 million tons, and 1.8 million tons, respectively, accounting for 33.5%, 39.7% and 26.8% of the total CE, respectively (Fig. 7). Advanced-IS cities encompass Chengdu and Panzhihua, with Chengdu exhibiting the highest CE (28.9%) – significantly surpassing that of Panzhihua. The majority of cities fall within the Medium-IS and Low-IS categories, with a noticeable disparity in CE within Medium-IS cities. Mianyang, the second-largest economy in Sichuan, contributes 9.3% to the province's CE, a figure higher than that of Ganzi (1.1%) and Aba City (1.5%). In contrast, the CE variance within Low-IS cities is considerably less, with Guangan yielding the highest CE (6.0%), and Bazhong the lowest (0.6%).

The Moran's I index of carbon emissions in Sichuan province in 2019 was -0.089. This indicates that the spatial distribution of urban carbon emissions has a certain negative correlation, that is, there is a tendency for carbon emission levels between adjacent cities to suppress each other. Spatially, low-carbon emission cities tend to be distributed around high-carbon emission cities, and vice versa. For instance, Chengdu, as the economic center and densely populated area of Sichuan province, has relatively high carbon emissions. However, in some surrounding cities, such as Ya'an and Meishan, due to the industrial structure mainly consisting of agriculture and some light industries, carbon emissions are relatively low, which reflects the negative correlation of carbon emissions between adjacent cities.

From the perspective of the z-score and p-value, the z-score is -0.68 and the p-value is 0.49. The Z-score is used to measure the significance of a statistic. The larger the absolute value, the more significant the result. The P value is used to test the null hypothesis, and generally, 0.05 is taken as the criterion for determining the significance level. In this case, the p-value is 0.49, which is much greater than 0.05, indicating that we cannot reject the null hypothesis. Therefore, from a statistical perspective, the spatial autocorrelation of urban carbon emissions in Sichuan province in 2019 is not significant (see Table 3).

Carbon Emissions Measurement Results of Cities

To authenticate the efficacy of the enhanced carbon emission measurement method proposed herein, we initially apply the traditional linear regression approach to quantify the relationship between city NTL-ISC and CE, as well as the relationship between NTL and CE. The linear regression results are shown in Table 4. Both NTL and the industrial structure coefficient pass the significance test, yielding an R^2 value of 0.89. Comparing the results of the unitary linear regression model established by NTL and CE ($R^2 = 0.87$), a notable improvement in precision is suggested. This verifies the

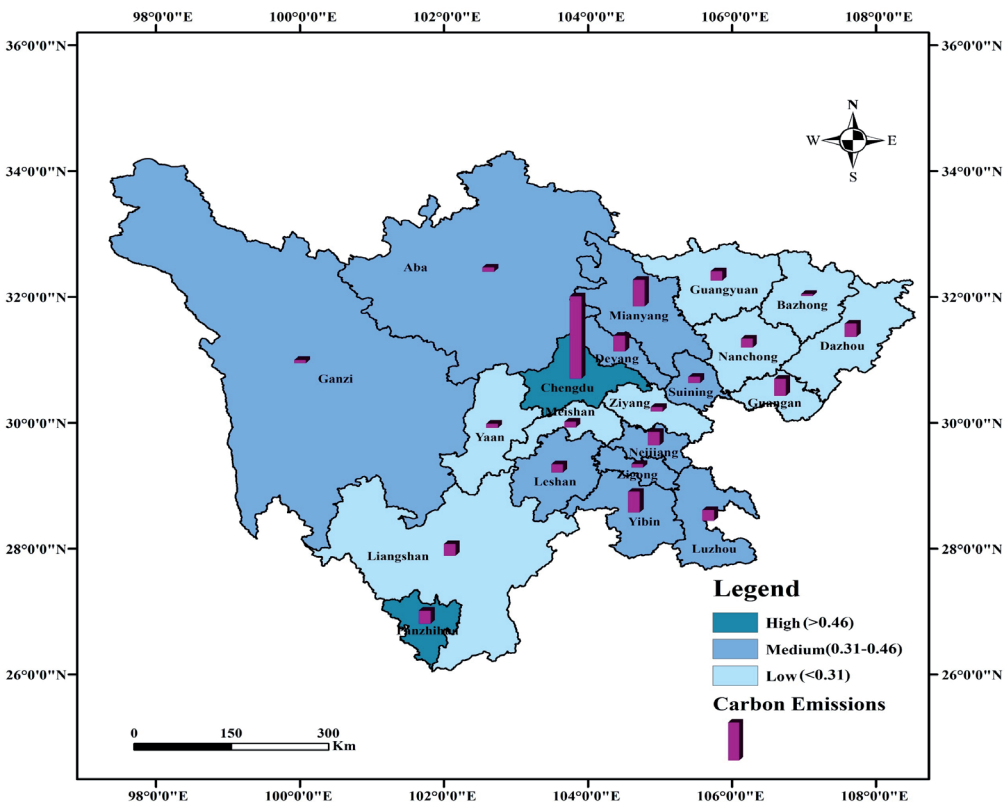

Fig. 6. Classification of the industrial structure of cities and carbon emissions distribution.

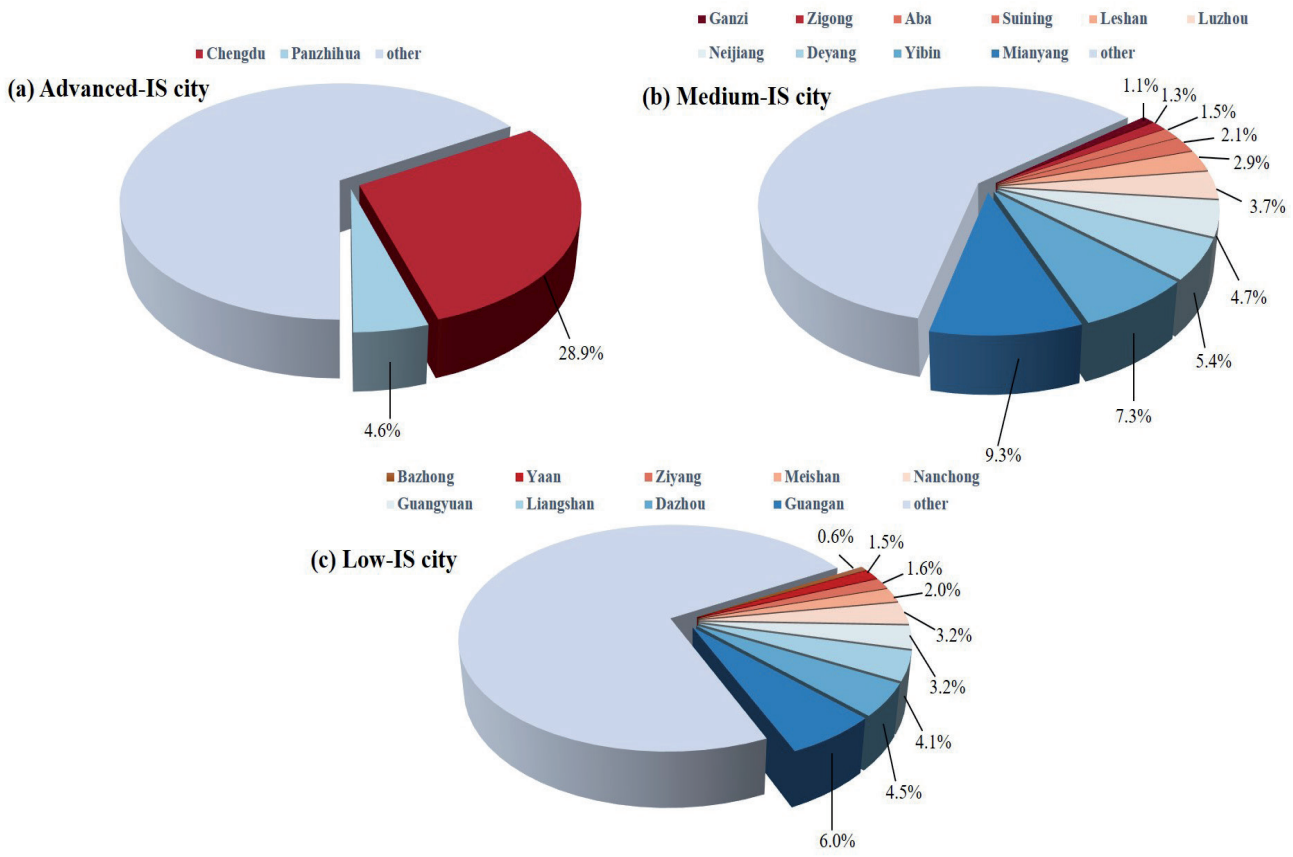

Fig. 7. CE of three kinds of industrial structure of cities.

Table 3. Spatial autocorrelation analysis.

Parameters	Value
Moran index	-0.089
Z score	-0.68
P value	0.49

Table 4. Regression model fitting results.

	City-scale CE (NTL-ISC)	City-scale CE (NTL)
NTL/	45.09*** (8.85)	50.66*** (12.09)
ISC/10^5	46.89* (1.76)	/
Constant/10^5	-17.20* (-2.02)	-3.72 (-0.95)
R^2	0.89	0.87
Adjusted R^2	0.88	0.86
F test	0	0
F	82.88	146.08

***p<0.01, **p<0.05, *p<0.1.

proposed coefficient of industrial structure's feasibility. NTL-ISC offers a more comprehensive depiction of city attributes, thereby better fitting the city-scale CE.

Building upon the foundations of traditional linear regression, this study employs the PSO-SVM model to establish the relationship between NTL, NTL-ISC, and city-scale CE, respectively. This method allows for a comparative analysis of the fitting results achieved through traditional linear regression, based on the fitting effectiveness of PSO-SVM. The findings indicate that the R^2 values of traditional linear regression and PSO-SVM, solely reliant on NTL, are 0.87 and 0.88, respectively, which are significantly lower than that of NTL-ISC (0.89 and 0.90) (Fig. 8). Meanwhile, the Root Mean Square Error (RMSE) values (1.26, 1.24) obtained by adding ISC were substantially lower than those garnered through using NTL alone (1.58, 1.49) (Fig. 8). This demonstrates that by incorporating ISC alongside NTL, can further characterize the difference of industrial structure between cities and paint a more accurate picture of city attributes. Thus, city-scale CE can be measured better, and the fitting performance of PSO-SVM is better than that of the traditional linear regression method.

Considering the variance in carbon emission volumes across cities, this research employs a measurement

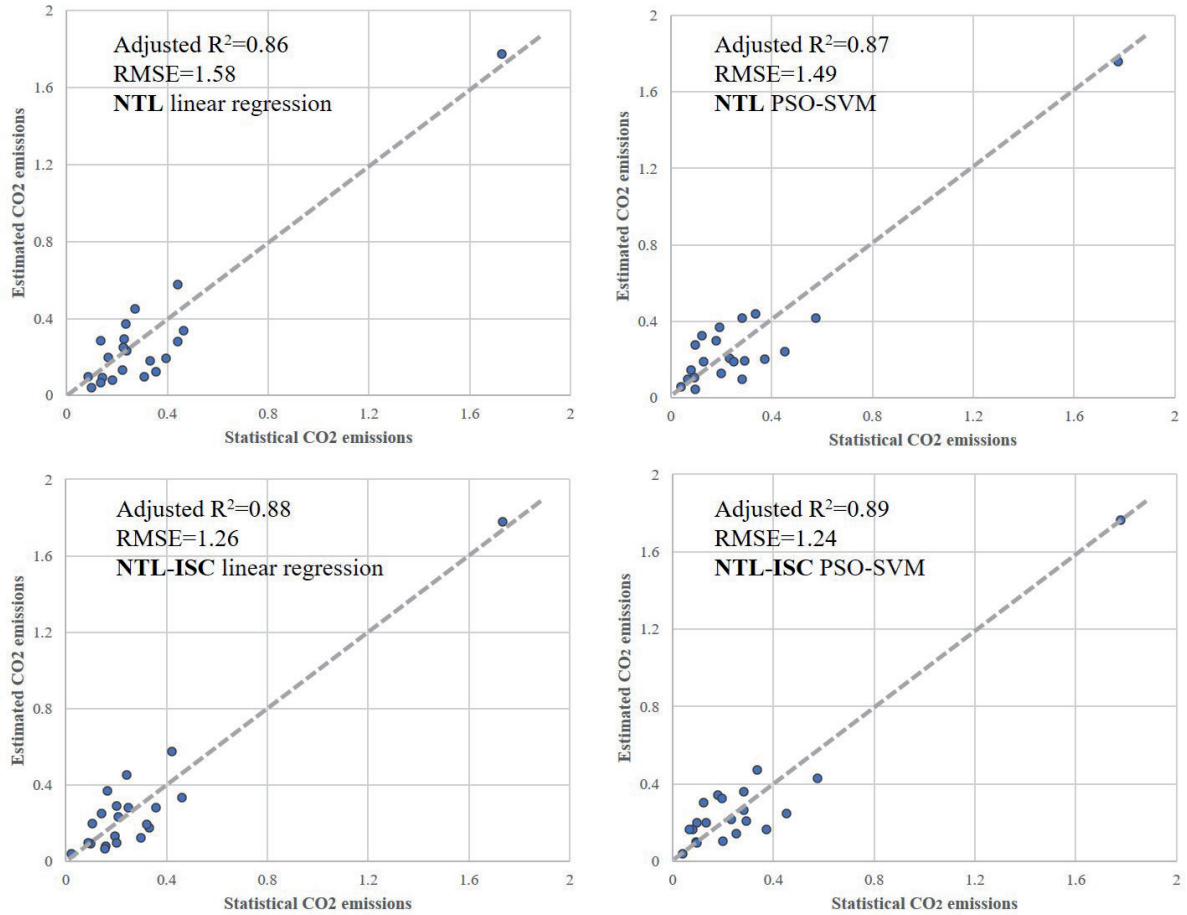

Fig. 8. Carbon emissions result assessment.

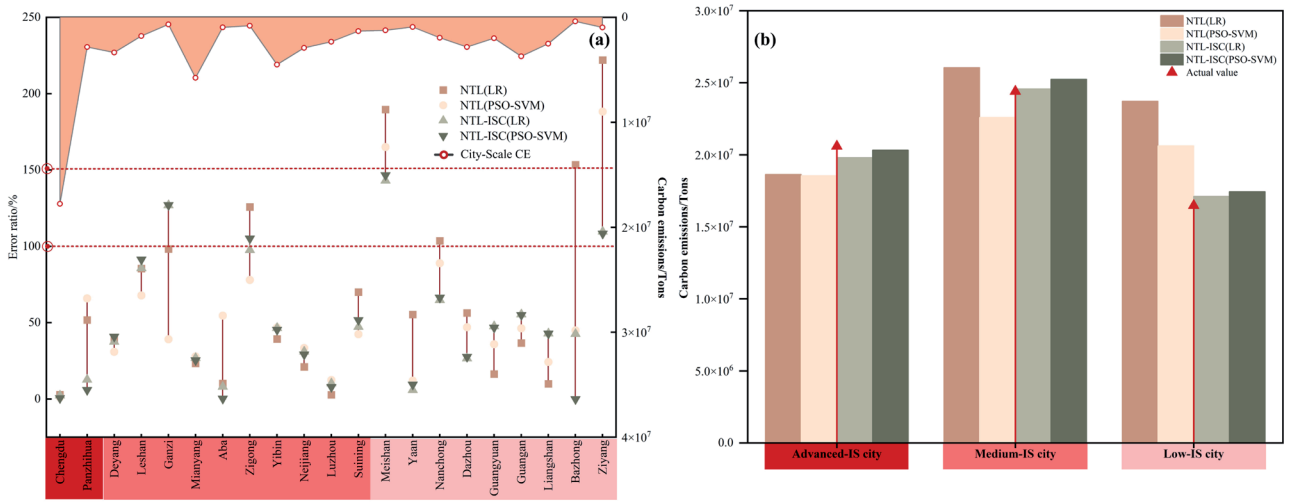

Fig. 9. City-scale and regional-scale CE measurement results.

error ratio to evaluate the efficacy of four distinct methodologies. Analysis of Fig. 9a) reveals that cities with lower carbon emission volumes exhibit a notably high error ratio in CE measurements derived from NTL, a discrepancy particularly pronounced in cities with a Low Industrial Structure (Low-IS) coefficient.

By further comparing the calculation results of total CE in Advanced-IS cities, Medium-IS cities, and Low-IS cities obtained by the four methods (Fig. 9b)), it can be seen that the calculation results of NTL-ISC are closer to the real value. NTL tends to underestimate the total CE for Advanced-IS cities and overestimates it for Medium-IS cities and Low-IS cities. This may be caused by defects in the NTL data itself. One of the main factors affecting the CE volume of a city is the carbon-intensive industries, which are usually located in sparsely populated areas, making it difficult to effectively estimate NTL [32]. Conversely, NTL-ISC can effectively measure CE at both urban and regional scales, which further highlights the validity of the NTL-ISC measurement method proposed in this paper.

Analysis of Carbon Emissions Intensity and Carbon Emissions Per Capita

Distribution of City-Scale CEC and CEI

In 2019, the average CEI and CEC in Sichuan Province were 0.13 t/1000 yuan and 0.75 t/person, respectively. Based on each city's CEI and CEC, the classification results obtained using the natural breakpoint method are presented in Fig. 10. CEI and CEC were predominantly higher in western regions and lower in eastern ones. Ganzi, Aba, and Panzhihua had

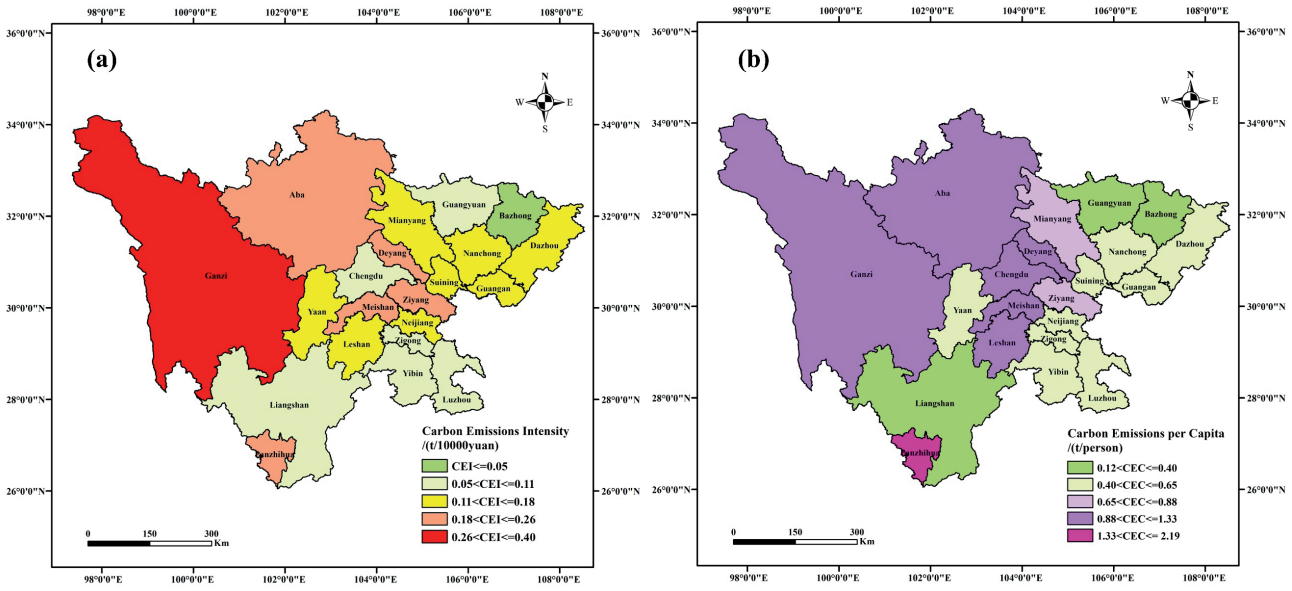

Fig. 10. Distribution characteristics of CEI and CEC of cities.

CEI values exceeding 0.13 t/10,000 yuan, with Ganzi displaying the most significant value at 0.40 t/10,000 yuan. Eastern cities, including Meishan, Deyang, and Ziyang, displayed relatively high CEI, with Ziyang presenting the highest CEI at 0.26 t/10,000 yuan. CEC in the Chengdu Plain Economic Zone and western regions was relatively high, with Panzhihua demonstrating the peak value of 2.19 t/person.

According to the ISC of cities calculated in City Industrial Structure Level and Characteristics of City-Scale Carbon Emissions, Chengdu and Panzhihua have a higher level of industrial structure. Nevertheless, the CEI of these two cities displayed contrary outcomes, a pattern also mirrored in their CEC. It is proven that there is no simple correlation between city CEI and CEC and the level of industrial structure.

Contribution Rate of Factors to CEI and CEC

The contribution rates of the tertiary industry, urbanization, and population density to CEI and CEC of 21 cities in Sichuan Province are shown in Fig. 11 and Fig. 12. The variance in CEI among Medium-IS cities was more prominent than that among Advanced-IS and Low-IS cities. Advanced-IS cities included Chengdu and Panzhihua, where the contribution rates of the tertiary industry, population density, and urbanization to Chengdu's CEI were 27%, 44%, and 28%, respectively, and for Panzhihua, they were 33%, 54%, and 14%. In Medium-IS cities, the contribution rate of population density varied considerably (0.8%-40%). It is notable that the contribution rate of population density in low-CEI cities was relatively high, that of the tertiary industry in high-CEI cities was substantial, and the contribution rate of urbanization remained relatively consistent, devoid of a discernible trend. For instance, in high-CEI cities: Ganzi (66%, 0.8%, 33%), low-CEI cities: Neijiang (31%, 40%, 29%). Compared with the other two types of cities, Low-IS cities have relatively concentrated contribution rates, with the tertiary industry taking up 35%-50%, urbanization and population density gathering in 35%-40% and 10%-35%, respectively. Low-CEI cities have a higher contribution rate of the tertiary industry, whereas high-CEI cities have a higher contribution rate of population density. For example: high-CEI city: Guangan (36%, 29%, 35%), low-CEI city: Liangshan (52%, 9%, 39%).

The contribution rate of tertiary industry, population density, and urbanization to CEC exhibited a pattern

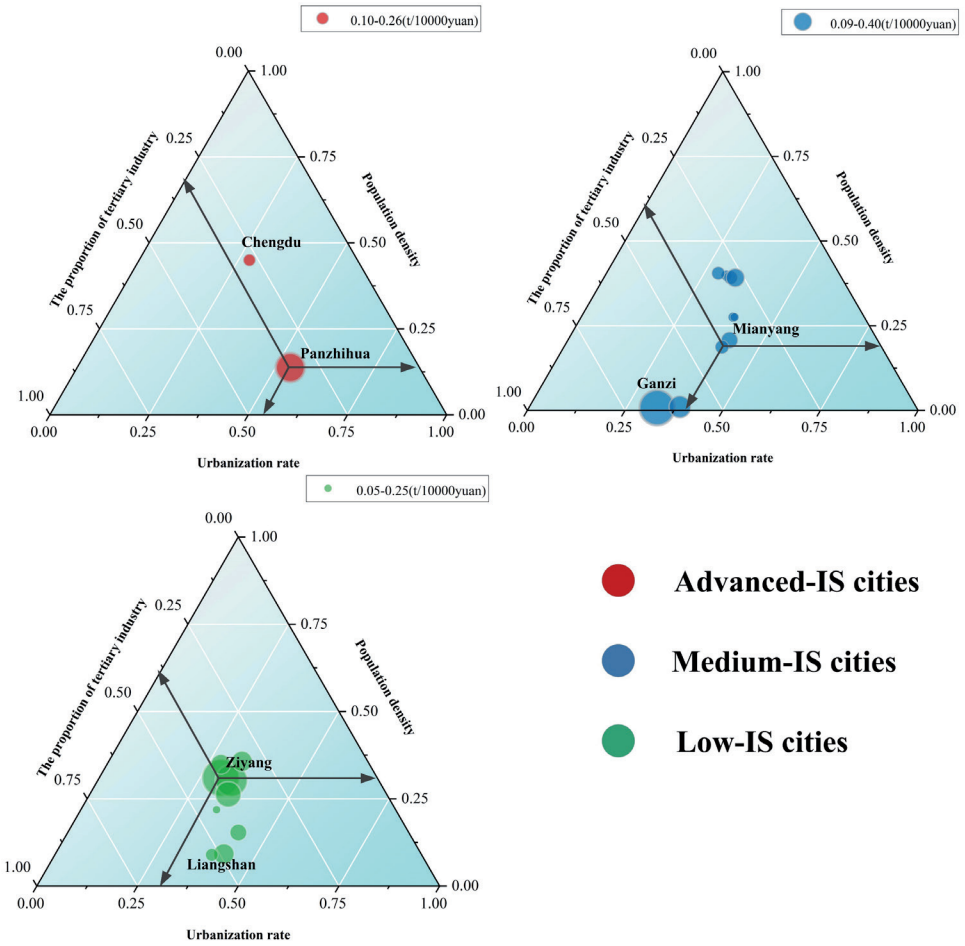

Fig. 11. Contribution rate of factors to CEI.

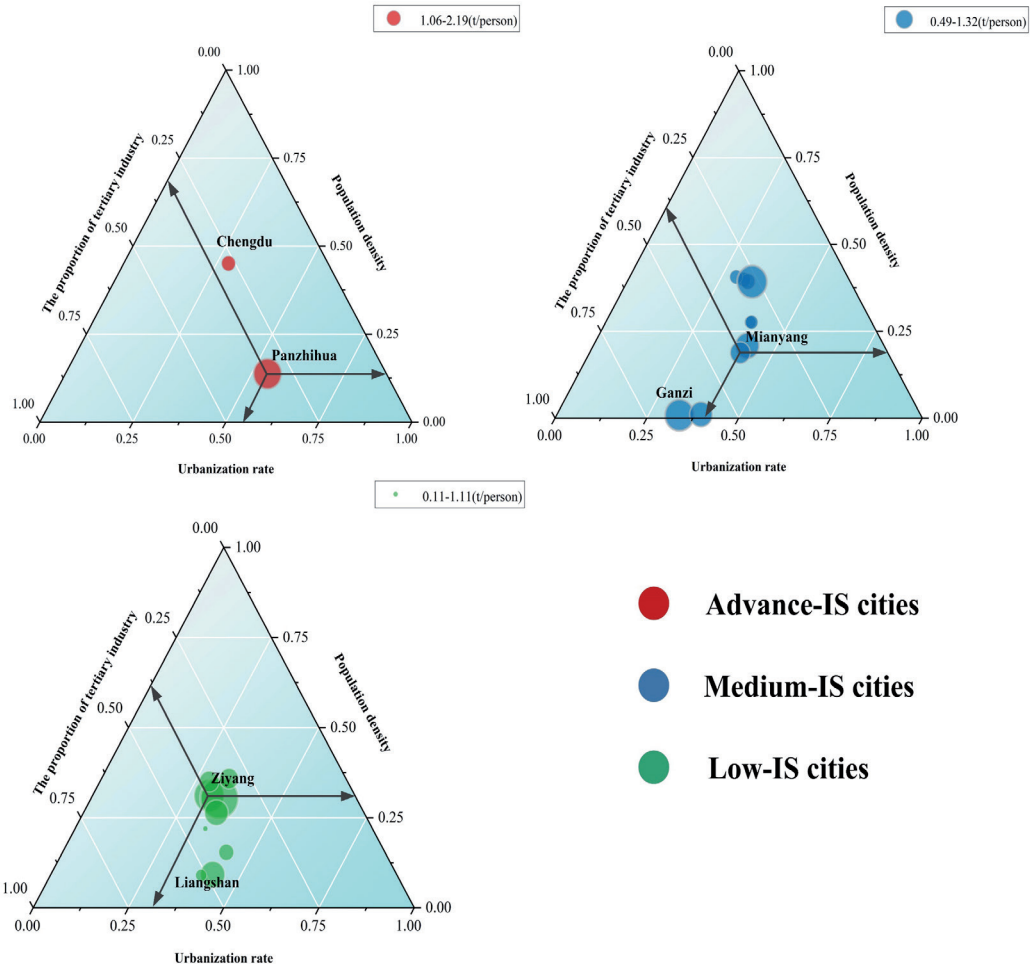

Fig. 12. Contribution rate of factors to CEC.

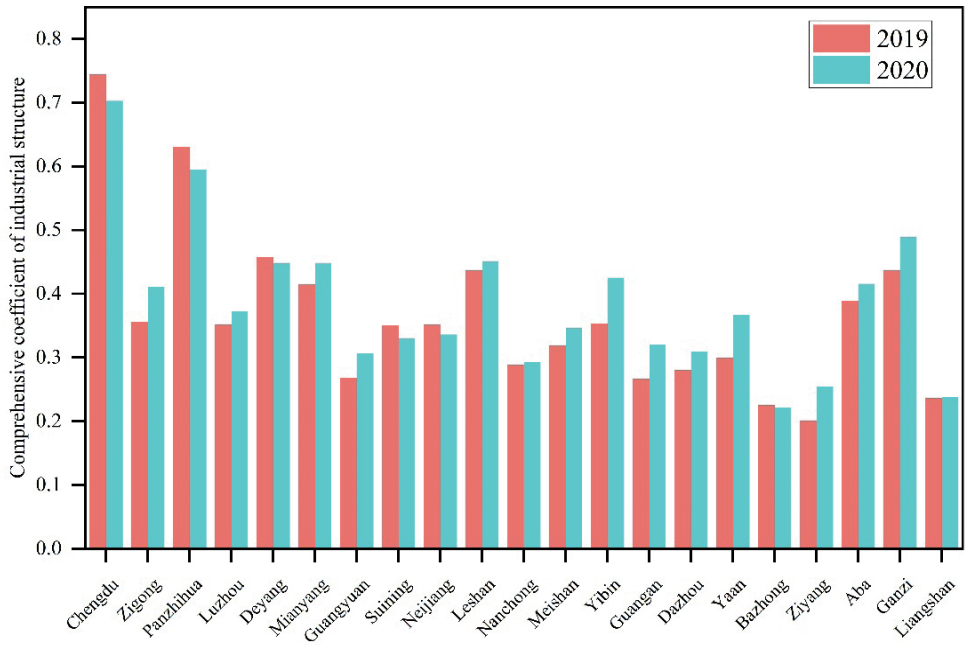

Fig. 13. Comparison of industrial structure coefficients in 2019 and 2020.

similar to that noted for CEI (Fig. 12). Specifically, the contribution ratio of tertiary industry to high-CEC cities in Medium-IS cities is higher; on the contrary, for Low-IS cities, low-CEC cities are higher. The contribution pattern of population density is inverse, meaning the contribution rate of high-CEC cities in Medium-IS cities is lower, while for high-CEC cities in Low-IS cities, it is higher.

Discussion

Verification of Measurement Method

Based on the collected 2020 industrial structure data for Sichuan Province, the ISC for its 21 cities (prefectures) was calculated using the methodology outlined in Materials and Methods (see Fig. 13).

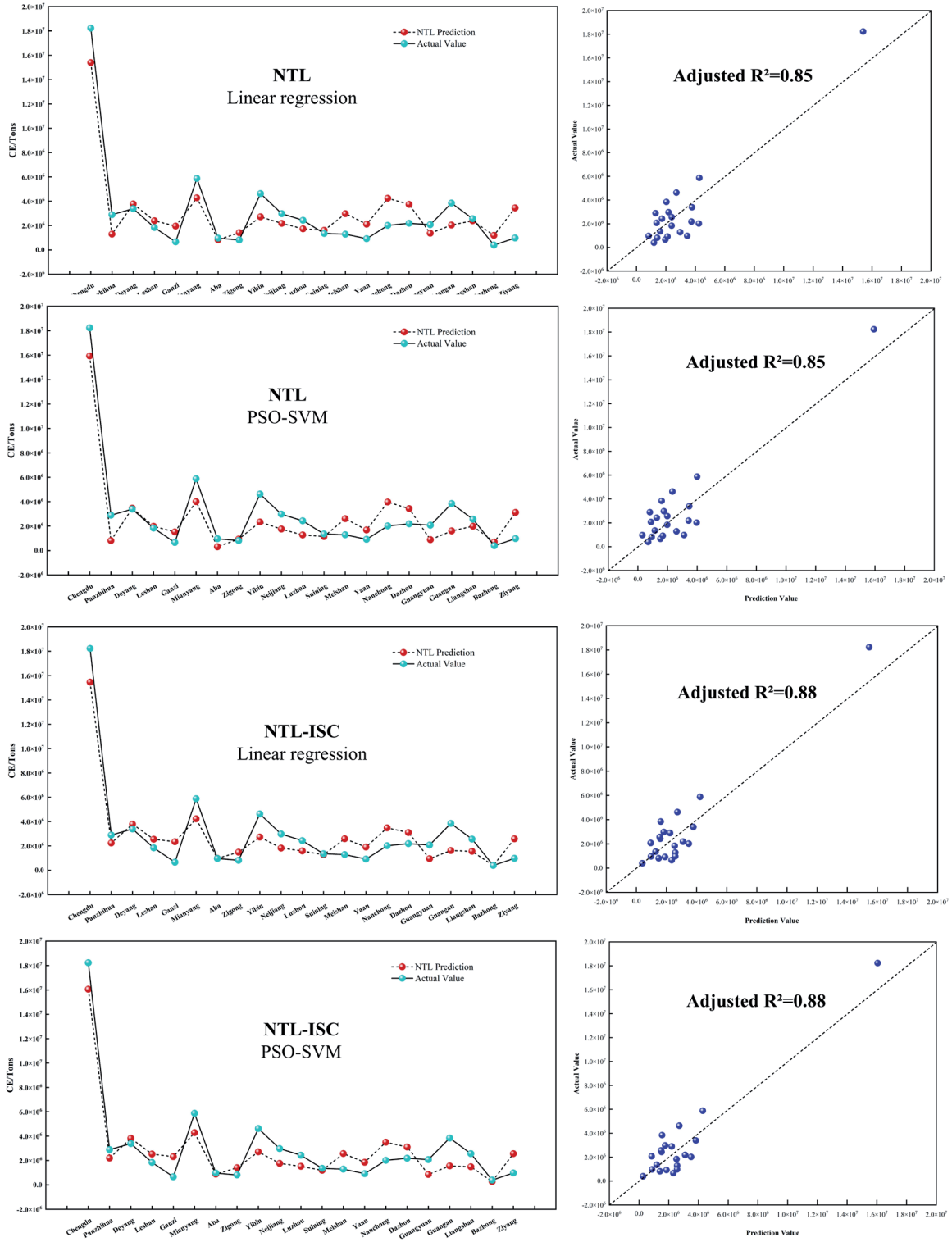

Fig. 14. Comparison between the estimated value and the true value in 2020.

A comparison of the ISC values between 2019 and 2020 reveals declines in cities including Chengdu, Panzhihua, Deyang, and Suining. This reduction can be primarily attributed to the advancement of the dual carbon goals policy post-2020, prompting greater emphasis on green and low-carbon development across regions, leading to restrictions and upgrades for energy-intensive and high-emission industries. Cities like Chengdu and Panzhihua accelerated their green industrial transitions, imposing constraints on high-energy-consumption and high-pollution sectors. However, the cultivation and growth of green emerging industries requires time, contributing to the observed decrease in their ISC in 2020. Furthermore, the outbreak of the COVID-19 pandemic in early 2020 resulted in strict containment measures. The postponement of business reopenings significantly disrupted production activities. In industrial cities like Deyang, the operating revenue of industrial enterprises above a designated size decreased, and the growth rate of industrial value-added slowed, adversely impacting secondary industry development and consequently reducing the ISC. In contrast, some cities experienced an increase in their ISC. This may be linked to labor force redistribution under the pandemic conditions.

This study extends its analysis by incorporating data from 2020 to further validate the proposed model, with findings detailed in the discussion section.

To verify the model's accuracy, data from 2020 was utilized, a year marked by China's announcement at the 75th United Nations General Assembly of its "dual carbon" goals aimed at fostering a green and low-carbon industrial transformation. To mitigate potential biases from national policy influences on the assessment coefficient weights of urban industrial structures, this analysis maintains the 2019 weights for evaluating urban industrial structures (Table 1). We calculated the CE for 21 cities and prefectures in Sichuan Province for 2020 using the annual average NTL and ISC values for 2020, as shown in Fig. 13.

The results of calculating city-scale CE using both the NTL and the NTL-ISC methods align closely with the actual trends. Furthermore, the estimated values demonstrate a strong correlation with the actual values, with R^2 values exceeding 0.85. The NTL-ISC method introduced in this study significantly enhances outcomes compared to those derived from NTL data alone, highlighting the effectiveness of incorporating urban industrial structure characteristics for a more accurate assessment of city-scale CE (Fig. 14).

Changes of Urban NTL under the Influence of COVID-19

As indicated in Verification of Measurement Method, the precision of both NTL and NTL-ISC measurements for 2020 has somewhat diminished, diverging from the actual city-scale CE values. A comparison of NTL data from 2019 to 2020 (Fig. 15) reveals a general decline in nighttime light intensity across most cities in Sichuan Province in 2020. This decrease aligns with findings from several studies linking a drop in urban

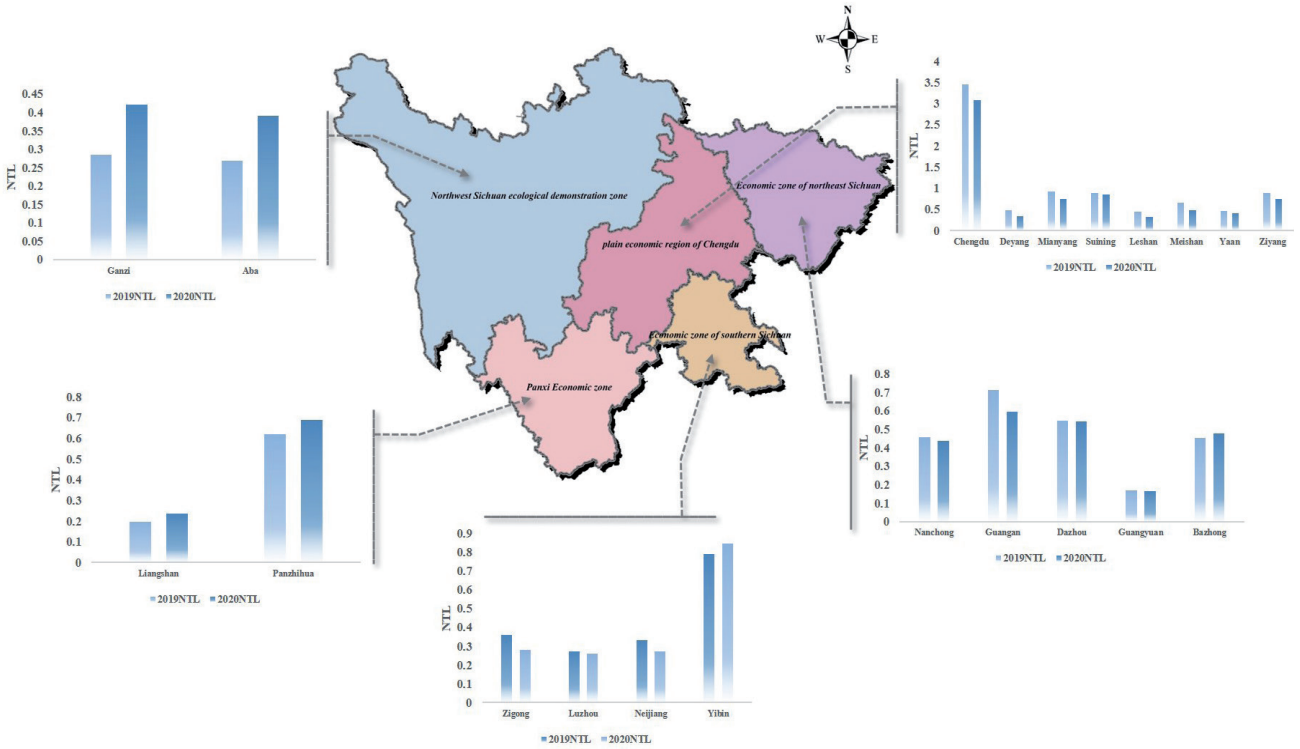

Fig 15. Comparison of NTL in 2019 and 2020 in Sichuan Province.

nighttime brightness to the COVID-19 outbreak [36-38]. Consequently, this paper delves into the specific impacts of COVID-19 on nighttime light data intensity across different economic regions of Sichuan Province.

The Chengdu Plain Economic Zone, including eight cities, has experienced a notable reduction in nighttime light intensity, averaging a 14.8% decline. Adjacent cities rely on this zone, centered around Chengdu City, as a pivotal hub for economic propulsion, making it the most dynamic region for economic activities within the province. The observed significant decrease in nighttime light intensity aligns with the hypothesis that large cities and their satellite towns tend to exhibit a marked reduction in nighttime brightness [39]. Conversely, the northeastern and southern economic zones of Sichuan experienced more modest declines in night light intensity, recording drops of 5.3% and 5.4%, respectively. These areas, primarily driven by secondary industries, exhibit less nighttime lighting due to the fact that night light intensity in industrial areas is relatively unaffected [39]. In an interesting shift, the COVID-19 pandemic has catalyzed population movements from major urban centers to rural, suburban, and smaller urban areas, leading to a pronounced increase in nighttime light intensity in the western regions of Sichuan, specifically the Northwest Sichuan Ecological Economic Zone and the Panxi Economic Zone, which saw increases of 45.5% and 13.8%, respectively.

This phenomenon suggests that the COVID-19 impact has, to some extent, affected the nighttime light intensity across various cities (Fig. 15), highlighting the susceptibility of NTL data to abrupt changes caused by emergencies or shifts in national policy. The COVID-19 impact significantly compromises the reliability of city-scale CE estimates based solely on NTL data, underscoring the efficacy of the NTL-ISC method introduced in this study.

There are still certain limitations in the research process. This paper takes Sichuan Province as the research area, and the number of urban samples is limited. In order to provide more appropriate carbon emission reduction suggestions for more cities with different industrial structure levels and prove the universality of the improvement methods proposed in this paper, it is necessary to collect more urban samples. Subsequently, we plan to improve future research in multiple aspects: Firstly, based on standards such as city size and industrial structure, collect more sample data of cities through statistical yearbooks, cooperative sharing and survey interviews; Secondly, optimize the measurement methods, combine life cycle assessment and input-output analysis, integrate multi-source data such as remote sensing and meteorology, and improve the model accuracy; Finally, based on this, suggestions are provided for cities with different levels of industrial structure, providing a scientific basis for policymakers and promoting cities to achieve carbon reduction and sustainable economic development.

Conclusions

Under the dual carbon goals, investigating urban-level carbon emission estimation methods is crucial for formulating effective carbon reduction policies. This study proposes an improved approach for directly utilizing NTL data to estimate urban carbon emissions. Considering the influence of industrial structure on urban energy consumption patterns, which may affect the representation capability of NTL for urban carbon emissions, this research employs NTL and ISC as independent variables. The PSO-SVM method is used to quantify the relationship between these variables and carbon emissions. The main conclusions are as follows:

(1) An industrial structure evaluation index system was established, incorporating the output value share, employment share, and labor productivity of both the secondary and tertiary industries. The entropy weight method was applied to determine indicator weights, and a weighted average yielded the urban ISC. Chengdu and Panzhihua exhibited the highest ISC values in Sichuan Province at 0.74 and 0.63, respectively, significantly exceeding those of other cities. Most cities fell within the medium-to-low range, indicating pronounced heterogeneity in industrial structure levels across Sichuan Province.

(2) The non-linear correlation between urban NTL, ISC, and statistical carbon emission data was modeled using PSO-SVM and compared with traditional regression methods. Results demonstrate that incorporating ISC significantly enhances the goodness-of-fit for both traditional regression models and PSO-SVM, while simultaneously reducing the error between actual and estimated carbon emission values. The integrated model combining NTL and urban industrial structure effectively mitigates the overestimation and underestimation issues observed in both the NTL-based LR model and the NTL-based PSO-SVM model, regardless of the underlying industrial structure level.

(3) Analysis of the contribution rates of tertiary industry share, urbanization rate, and population density to CEI and CEC reveals similar patterns for both CEI and CEC. Population density exhibits a higher contribution rate in Medium-IS cities characterized by low-to-medium CEI or low CEC, while its contribution is higher for cities with high CEI or high CEC within the Low-IS category. Conversely, the contribution pattern of the tertiary industry share is inverse to that of population density. The urbanization rate shows a relatively high contribution (54%) in Panzhihua; its contribution in other cities is relatively concentrated with minimal variation.

Acknowledgements

The authors declare that no funds, grants, or other support were received during the preparation of this manuscript.

Conflict of Interest

The authors declare that they have no known competing financial interests or personal relationships that could have appeared to influence the work reported in this paper.

Author Contributions

Wenfeng Huang: Conceptualization, Methodology, Validation, Writing – original draft. Xiaoyu Zhang: Methodology, Supervision, Writing – review & editing. Ke Pan: Software, Writing – review & editing, Data curation. Jie Luo: Visualization, Formal analysis. Hao Tang: Methodology, Software.

References

1. SUFYANULLAH K., AHMAD K.A., ALI M.A.S. Does emission of carbon dioxide is impacted by urbanization? An empirical study of urbanization, energy consumption, economic growth and carbon emissions-Using ARDL bound testing approach. Energy Policy. **164**, 112908, **2022**.
2. SHAN Y., FANG S., CAI B., ZHOU Y., LI D., FENG K., HUBACEK K. Chinese cities exhibit varying degrees of decoupling of economic growth and CO_2 emissions between 2005 and 2015. One Earth. **4** (1), 124, **2021**.
3. HUO T., LI X., CAI W., ZUO J., JIA F., WEI H. Exploring the impact of urbanization on urban building carbon emissions in China: Evidence from a provincial panel data model. Sustainable Cities and Society. **56**, 102068, **2020**.
4. WU S., HU S., FRAZIER A.E., HU Z. China's urban and rural residential carbon emissions: past and future scenarios. Resources, Conservation and Recycling. **190**, 106802, **2023**.
5. VERMA P., KUMARI T., RAGHUBANSHI A.S. Energy emissions, consumption and impact of urban households: A review. Renewable and Sustainable Energy Reviews. **147**, 111210, **2021**.
6. PU Y., WANG Y., WANG P. Driving effects of urbanization on city-level carbon dioxide emissions: From multiple perspectives of urbanization. International Journal of Urban Sciences. **26** (1), 108, **2022**.
7. ZHENG Y., YANG H., HUANG J., CUI Q., ZHAN J. Industrial agglomeration measured by plants' distance and CO_2 emissions: Evidence from 268 Chinese prefecture-level cities. Technological Forecasting and Social Change. **176**, 121469, **2022**.
8. WANG Z., LI X., MAO Y., LI L., WANG X., LIN Q. Dynamic simulation of land use change and assessment of carbon storage based on climate change scenarios at the city level: A case study of Bortala, China. Ecological Indicators. **134**, 108499, **2022**.
9. ZHAO C., CAO X., CHEN X., CUI X. A consistent and corrected nighttime light dataset (CCNL 1992–2013) from DMSP-OLS data. Scientific Data. **9** (1), 424, **2022**.
10. DU X., SHEN L., WONG S.W., MENG C., YANG Z. Night-time light data based decoupling relationship analysis between economic growth and carbon emission in 289 Chinese cities. Sustainable Cities and Society. **73**, 103119, **2021**.
11. ORTAKAVAK Z., ÇABUK S.N., CETIN M., SENYEL KURKCUOGLU M.A., CABUK A. Determination of the nighttime light imagery for urban city population using DMSP-OLS methods in Istanbul. Environmental monitoring and assessment. **192** (12), 790, **2020**.
12. FARUOLO M., FALCONIERI A., GENZANO N., LACAVA T., MARCHESE F., PERGOLA N. A daytime multisensor satellite system for global gas flaring monitoring. IEEE Transactions on Geoscience and Remote Sensing. **60**, 1, **2022**.
13. WANG L., ZHANG N., DENG H., WANG P., YANG F., QU J.J., ZHOU X. Monitoring urban carbon emissions from energy consumption over China with DMSP/OLS nighttime light observations. Theoretical and Applied Climatology. **149** (3), 983, **2022**.
14. ZHENG Y., FAN M., CAI Y., FU M., YANG K., WEI C. Spatio-temporal pattern evolution of carbon emissions at the city-county-town scale in Fujian Province based on DMSP/OLS and NPP/VIIRS nighttime light data. Journal of Cleaner Production. **442**, 140958, **2024**.
15. CHEN J., GAO M., CHENG S., HOU W., SONG M., LIU X., LIU Y., SHAN Y. County-level CO_2 emissions and sequestration in China during 1997-2017. Scientific Data. **7** (1), 391, **2020**.
16. ZHENG Y., FAN M., CAI Y., FU M., YANG K., WEI C. Spatio-temporal pattern evolution of carbon emissions at the city-county-town scale in Fujian Province based on DMSP/OLS and NPP/VIIRS nighttime light data. Journal of Cleaner Production. **442**, 140958, **2024**.
17. WEI G., HE B. J., SUN P., LIU Y., LI R., OUYANG X., LI S. Evolutionary trends of urban expansion and its sustainable development: Evidence from 80 representative cities in the belt and road initiative region. Cities. **138**, 104353, **2023**.
18. RICKWOOD P., GLAZEBROOK G., SEARLE G. Urban structure and energy – a review. Urban Policy and Research. **26** (1), 57, **2008**.
19. SHI K., SHEN J., WU Y., LIU S., LI L. Carbon dioxide (CO_2) emissions from the service industry, traffic, and secondary industry as revealed by the remotely sensed nighttime light data. International Journal of Digital Earth. **14** (11), 1514, **2021**.
20. LIU F. The impact of China's low-carbon city pilot policy on carbon emissions: based on the multi-period DID model. Environmental Science and Pollution Research. **30** (34), 81745, **2023**.
21. ZENG S., JIN G., TAN K., LIU X. Can low-carbon city construction reduce carbon intensity? Empirical evidence from low-carbon city pilot policy in China. Journal of Environmental Management. **332**, 117363, **2023**.
22. LI L., LEI Y., WU S., HE C., CHEN J., YAN D. Impacts of city size change and industrial structure change on CO_2 emissions in Chinese cities. Journal of Cleaner Production. **195**, 831, **2018**.
23. ZHU B., SHAN H. Impacts of industrial structures reconstructing on carbon emission and energy consumption: A case of Beijing. Journal of Cleaner Production. **245**, 118916, **2020**.
24. YU B. Urban spatial structure and total-factor energy efficiency in Chinese provinces. Ecological Indicators. **126**, 107662, **2021**.
25. WU J., LIU C., GUO H., LI P., SUN W. Examining intra-city carbon budget and carbon balance zoning

based on firm-level big data: A case study of Nanjing, China. Ecological Indicators. **166**, 112304, **2024**.
26. ZHENG Y., FAN M., CAI Y., FU M., YANG K., WEI C. Spatio-temporal pattern evolution of carbon emissions at the city-county-town scale in Fujian Province based on DMSP/OLS and NPP/VIIRS nighttime light data. Journal of Cleaner Production. **442**, 140958, **2024**.
27. CHEN X., MA W., VALDMANIS V. Can labor productivity growth reduce carbon emission? Evidence from OECD countries and China. Management of Environmental Quality: An International Journal. **33** (3), 644, **2021**.
28. PAN X., GUO S., XU H., TIAN M., PAN X., CHU J. China's carbon intensity factor decomposition and carbon emission decoupling analysis. Energy. **239**, 122175, **2022**.
29. ZHE W., XIGANG X., FENG Y. An abnormal phenomenon in entropy weight method in the dynamic evaluation of water quality index. Ecological Indicators. **131**, 108137, **2021**.
30. YANG S., YANG X., GAO X., ZHANG J. Spatial and temporal distribution characteristics of carbon emissions and their drivers in shrinking cities in China: Empirical evidence based on the NPP/VIIRS nighttime lighting index. Journal of Environmental Management. **322**, 116082, **2022**.
31. SHI K., SHEN J., WU Y., LIU S., LI L. Carbon dioxide (CO_2) emissions from the service industry, traffic, and secondary industry as revealed by the remotely sensed nighttime light data. International Journal of Digital Earth. **14** (11), 1514, **2021**.
32. YANG D., LUAN W., QIAO L., PRATAMA M. Modeling and spatio-temporal analysis of city-level carbon emissions based on nighttime light satellite imagery. Applied Energy. **268**, 114696, **2020**.
33. EL AMOURY S., SMILI Y., FAKHRI Y. Design of an Optimal Convolutional Neural Network Architecture for MRI Brain Tumor Classification by Exploiting Particle Swarm Optimization. Journal of Imaging. **11** (2), 31, **2025**.
34. Data and statistics. Available online: https://www.iea.org/data-and-statistics (accessed on April 1, 2025).
35. ZHOU Y., CHEN M., TANG Z., ZHAO Y. City-level carbon emissions accounting and differentiation integrated nighttime light and city attributes. Resources, Conservation and Recycling. **182**, 106337, **2020**.
36. JECHOW A., HÖLKER F. Evidence that reduced air and road traffic decreased artificial night-time skyglow during COVID-19 lockdown in Berlin, Germany. Remote Sensing. **12** (20), 3412, **2020**.
37. XU G., XIU T., LI X., LIANG X., JIAO L. Lockdown induced night-time light dynamics during the COVID-19 epidemic in global megacities. International Journal of Applied Earth Observation and Geoinformation. **102**, 102421, **2021**.
38. YIN R., HE G., JIANG W., PENG Y., ZHANG Z., LI M., GONG C. Night-time light imagery reveals China's city activity during the COVID-19 pandemic period in early 2020. IEEE Journal of Selected Topics in Applied Earth Observations and Remote Sensing. **14**, 5111, **2021**.
39. PAVLAČKA D., VYVLEČKA P., BARVÍŘ R., RYPL O., BURIAN J. Influence of COVID-19 on night-time lights in Czechia. Journal of Maps. **19** (1), 2235381, **2023**.